Marine and Petroleum Geology 137 (2022) 105494

Contents lists available at ScienceDirect

Marine and Petroleum Geology

journal homepage: www.elsevier.com/locate/marpetgeo

Modelling the dynamic response of shallow methane hydrates to simultaneous sea level and bottom water temperatures variations since the last glacial maximum on the Amazon Deep-Sea Fan, Brazil

Rafael Braga [a], Felipe Dalla Vecchia [a,b,c], Rodrigo Sebastian Iglesias [a,b,c,*]

[a] Instituto do Petróleo e dos Recursos Naturais – PUCRS – Pontifícia Universidade Católica do Rio Grande do Sul, 90619-900, Porto Alegre, RS, Brazil
[b] Escola Politécnica – PUCRS – Pontifícia Universidade Católica do Rio Grande do Sul, 90619-900, Porto Alegre, RS, Brazil
[c] Programa de Pós-Graduação em Engenharia e Tecnologia de Materiais – PUCRS – Pontifícia Universidade Católica do Rio Grande do Sul, 90619-900, Porto Alegre, RS, Brazil

ARTICLE INFO

Keywords:
Methane hydrates
TOUGH+HYDRATE
Amazon fan
Last glacial maximum

ABSTRACT

In marine sediments, methane hydrate can occur within the methane hydrate stability zone (MHSZ), which extends from the seafloor to a certain depth below it, within which the conditions of pressure and temperature are such that allow their formation and stability. Variations in sea level and in bottom water temperatures (BWTs) have opposite effects on the stability zone: a sea level rise leads to higher hydrostatic pressure, which tends to enlarge the MHSZ, while an increase in temperature tends to shrink it, and vice-versa. When the MHSZ shrinks, methane hydrate dissociates, releasing water and gaseous methane into the sediment pores. If the gaseous methane reaches the seafloor, it will be released into the ocean. In this study, we use numerical modelling to investigate the dynamic response of shallow methane hydrates at 550, 575, 600, 625, 650, 700 and 750 m water depth (mwd), on the Amazon Deep-Sea Fan, Equatorial Atlantic Ocean (near the northern coast of Brazil), to simultaneous sea level and BWTs increases, since the Last Glacial Maximum (LGM) up to the present. These water depths lie on the feather edge of the MHSZ, where hydrates are most sensitive to pressure and temperature perturbations. The results suggest that the methane hydrate stability decrease caused by the BWTs increases has completely overcome the increase in stability owing to sea level increase, for 550 and 575 mwd. For these two water depths, the MHSZ disappeared in the models and all the hydrate initially present has dissociated. The modelling results indicate that gaseous methane started to be released into the ocean at ca. 17,500 y BP for 550 mwd and at ca. 16,000 y BP for 575 mwd. For the other water depths considered, hydrate stability decrease caused by the BWT increase has only partly overcome the increase in stability due to pressure increase, so that the MHSZs have shrank, but have not totally disappeared in the models. Gaseous methane was released into the ocean from ca. 14,000 y BP to 7000 y BP for 600 mwd. For 625, 650, 700 and 750 mwd, no gaseous methane has been released into the ocean. Methane release amounts and flowrates are maximum limits for each depth, as no methane consumption processes, such as anaerobic oxidation, are modeled in this study.

1. Introduction

Methane hydrates are solid crystalline compounds in which the gas molecules are trapped within cavities (or cages) formed by water molecules. In nature, they occur in the permafrost and in oceanic sediments, where the high pressure and low temperature conditions, together with the availability of water and gas, allow their formation and stability (Sloan, 2003; Tréhu et al., 2006; Hester and Brewer, 2009).

In marine sediments, the depth interval where methane hydrates are stable is known as the methane hydrate stability zone (MHSZ). It extends from the seafloor to a certain depth below it, that coincides with the depth in which the methane hydrate stability curve intersects the regional geothermal gradient (e.g., Tréhu et al., 2006; Hester and Brewer, 2009). The MHSZ thickness is controlled by water depth, bottom water temperature, geothermal gradient, salinity and gas composition (e.g., Darnell and Flemings, 2015 and references therein), ranging from a few meters to hundreds, depending on these parameters. Changes

* Corresponding author. Instituto do Petróleo e dos Recursos Naturais – PUCRS – Pontifícia Universidade Católica do Rio Grande do Sul, 90619-900, Porto Alegre, RS, Brazil.
E-mail address: rodrigo.iglesias@pucrs.br (R.S. Iglesias).

https://doi.org/10.1016/j.marpetgeo.2021.105494
Received 11 May 2021; Received in revised form 9 December 2021; Accepted 16 December 2021
Available online 18 December 2021

Nomenclature

AOM	Anaerobic oxidation of methane
BWTs	Bottom water temperatures
LGM	Last Glacial Maximum (20,000 y BP)
mbsf	meters below the seafloor
MHSZ	Methane hydrates stability zone
MTDs	Mass-transport deposits
mwd	meters water depth
SA	Aqueous phase saturation
SH	Hydrate saturation
λ_{dry}	"Dry" thermal conductivity
λ_{wet}	"Wet" thermal conductivity (under fully water-saturated conditions)
SRZ	Sulfate reduction zone
y BP	years before present

in sea level (pressure) and/or in bottom water temperatures (BWTs) may increase or reduce the MHSZ: a sea level increase promotes an enlargement of the MHSZ, while an increase in BWTs reduces its size, and vice-versa. These variations occur during glacial/interglacial cycles, with sufficient range to destabilize gas hydrate accumulations during deglaciation periods. It has been suggested that methane amounts released to the atmosphere during deglaciation could be sufficient to impact the deglaciation rates, by enhancing the greenhouse effect and global warming (Paull et al., 1991). Changes in the MHSZ are also linked to temperature increase from recent climate change (Ketzer et al., 2020; Phrampus and Hornbach, 2012; Reagan and Moridis, 2007, 2008; Stranne et al., 2016a,b).

When the stability zone is reduced, methane hydrate dissociate, releasing water and gaseous methane in the sediment pores; if this gaseous methane migrates upward and reaches the seafloor, it will be released into the ocean. However, a significant part of the methane released during hydrates dissociation may not reach the seafloor, due to methane and sulfate consumption by the anaerobic oxidation of methane (AOM), that takes place within the sulfate reduction zone (SRZ). The SRZ extends from the seafloor to a certain depth below it – usually a few meters, but its thickness may vary significantly (Hunter et al., 2013 and references therein; Stranne et al., 2019 and references therein). The AOM is considered a microbial filter for marine methane (Egger et al., 2018; Stranne et al., 2019). As reported by Stranne et al. (2019), in a global scale, more than 90% of the methane produced in ocean sediments is consumed by AOM.

Several modelling studies have been carried out to investigate changes in the MHSZ, methane hydrates dissociation and gas release into the ocean. In general, these studies assessed the effects of BWTs increases driven by climate change and/or seasonal BWTs oscillations on methane hydrate dissociation and gas release into the ocean, over periods of decades or centuries (Reagan and Moridis, 2008; Reagan et al., 2011; Thatcher et al., 2013; Marín-Moreno et al., 2013, 2015a, 2015b; Stranne et al., 2016a,b, 2019; Stranne, O'Regan and Jakobsson, 2016, 2017; Braga et al., 2020). Due to the time scales considered in these studies, the sea level was considered constant (i.e., constant pressure). There is a lack of published studies that investigate the effects of simultaneous sea level (pressure) and BWTs increases on methane hydrate stability, considering heat and mass fluxes within a multiphase and multicomponent approach. Xu, Lowell and Peltzer (2001) used a mathematical model and numerical simulations to address this issue, but they assessed the effects of pressure and temperature variations separately. Hunter et al. (2013) used a mathematical model to assess the effects of BWTs variations along with linear sea level increases on the future evolution of the global hydrate stability zone volume and hydrate inventory. Although they considered BWTs and sea level variations together, they focused on centennial time scales (from ~1950 to ~2850); furthermore, their mathematical model did not account for phase changes and fluxes within the sediments pores and some important phenomena were disregarded (e.g., pore water freshening after hydrate dissociation, latent heat, solubility changes due to local changes in pressure, temperature and salinity, and hydrate formation). Most of these modeling studies do not evaluate the AOM impact on methane release into the ocean, neither geomechanical effects on the system. An early attempt is the work by Stranne et al. (2019), that incorporates an AOM module to the TOUGH + HYDRATE code including geomechanics (Moridis, 2014; Stranne et al., 2017), adding a sink for methane from dissolved hydrates. Results highlight the complex interplay between the AOM rate and methane flow regime through the sulfate reduction zone, with fracture flow reducing AOM capacity.

In this work, we investigate the effects of simultaneous sea level (pressure) and BWTs increases on methane hydrate stability and on gaseous methane release into the ocean, since the Last Glacial Maximum [LGM – 20,000 years before present (y BP)] up to the present. To do so, we performed numerical simulations with the TOUGH + HYDRATE v1.5 code (Moridis, 2014). Geochemical or geomechanical effects on the system (AOM or other methane sinks, and fracture flow) are not considered in these simulations. The models consisted seven vertical (1D) models at 550, 575, 600, 625, 650, 700 and 750 m water depth (mwd), representative of a shallow region on the Amazon Deep-Sea Fan, Amazonas Basin, Equatorial Atlantic Ocean, Brazil (Fig. 1). The Amazon Fan occupies an area of ca. 330,000 km^2, covering water depths of over 4000 m (Ketzer et al., 2018). The presence of giant mass-transport deposits (MTDs) is a significant feature of the region, that has been linked to gas hydrates dissociation and/or variations in sedimentation rates in the past (Maslin et al., 2005). Recently, gas hydrates (predominantly methane) have been recovered on different areas on the Amazon Fan, and several gas plumes have been detected in the water column, venting on the seafloor, from 650 to 2600 mwd (Ketzer et al., 2018). The plumes between 650 and 715 mwd may be related to methane hydrates dissociation, since this range of water depths are within the current feather edge of the MHSZ on the Amazon Fan (Ketzer et al., 2018, 2019) (Fig. 1). The feather edge of the MHSZ refers to its up-dip limit on the continental slopes, where the MHSZ thins to vanishing at the seafloor (Ketzer et al., 2019 and references therein). This is the part of the slope most sensitive to seafloor temperature perturbations (Stranne et al., 2016) and, therefore, it is where methane hydrate is most sensitive.

2. Modelling approach

The numerical simulations were performed with the TOUGH + HYDRATE v1.5 code (T + H), a numerical code for the simulation of the behavior of CH_4-hydrate-bearing systems. In the current version of T + H, only methane hydrates are considered (no other hydrocarbon components are included). T + H includes an equilibrium and a kinetic model for hydrates formation and dissociation, and accounts for heat and up to four mass components (water, methane, water-soluble inhibitors and hydrate), that are partitioned among four possible phases (aqueous phase, gas phase, ice phase and hydrate phase) (Moridis, 2014).

The basic 1D model used consists in a column of 1.0 × 1.0 x 1000 m in the (x, y, z) directions, respectively, as depicted in Fig. 2a. Fluxes can occur only in the z direction, that represents the depth below the seafloor. The model has 4001 cells of 0.25 m height ($dz = 0.25$ m) and 1 cell of 1.0 mm height ($dz = 0.001$ m) at the top, which is the top boundary and represents the seafloor. For all the 4002 cells, $dx = dy = 1.0$ m, so that the cells have a surface area of 1.0 m^2 (Fig. 2a).

We used this model in seven water depths, 550, 575, 600, 625, 650, 700 and 750 m (Fig. 2b), to cover the water depth range of the current feather edge of the MHSZ, which is estimated by Ketzer et al. (2019) to lie between 500 and 670 mwd. The initial conditions for each 1D model refer to the conditions at the LGM. In these conditions (which will be

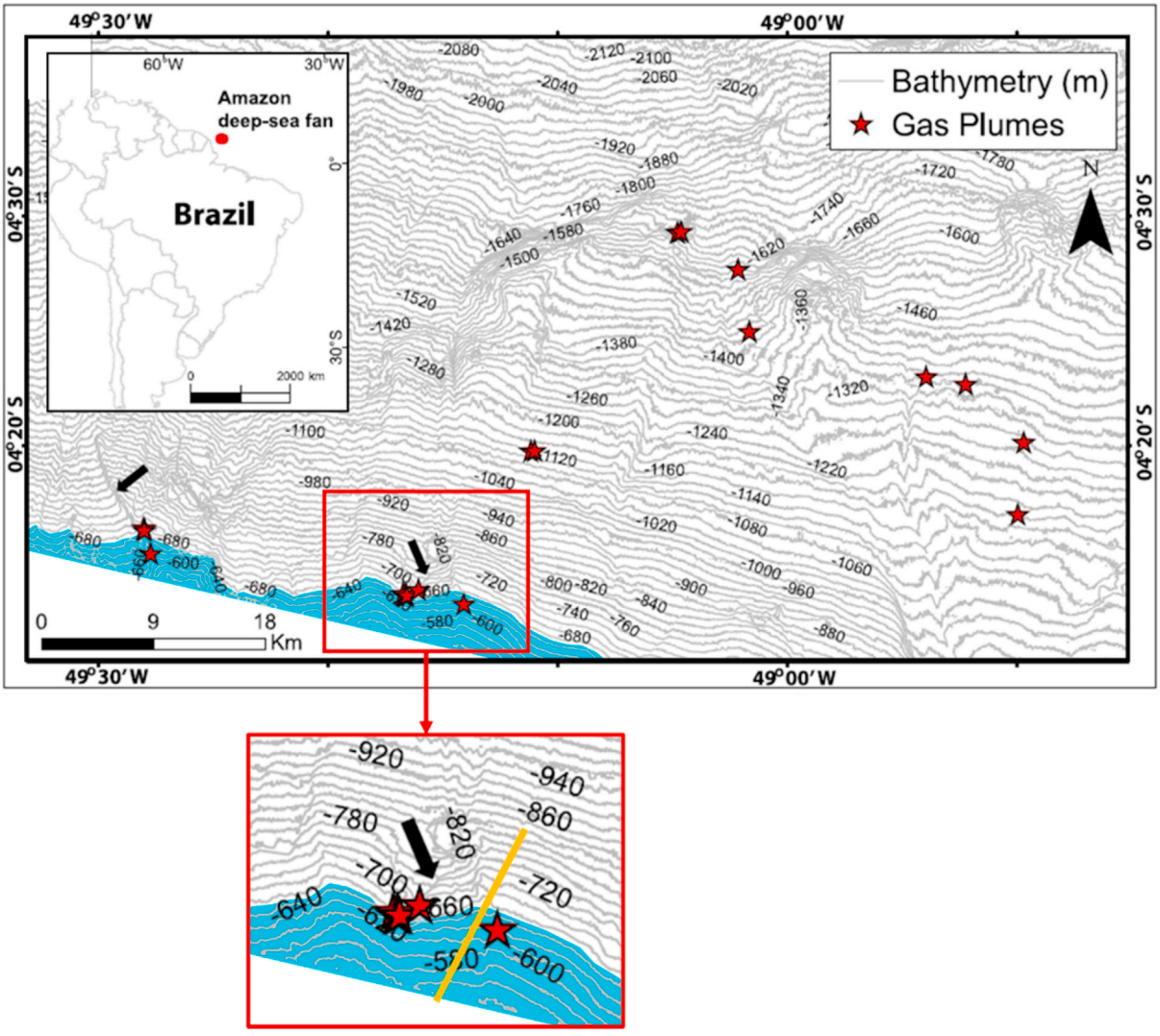

Fig. 1. Location of the study area of this work (red rectangle) on the Amazon Deep-Sea Fan, and the transect considered (yellow line). The red stars are the gas plumes detected in the water column and the light blue shaded area indicates the depth range of the current feather edge of the MHSZ estimated by Ketzer et al. (2019) to be between 500 and 670 mwd. Adapted from Ketzer et al. (2019). (For interpretation of the references to colour in this figure legend, the reader is referred to the Web version of this article.)

further explained), there would be no methane hydrates at 500 and 525 mwd.

The input parameters and properties for the model are summarized in Table 1. Water salinity and sediment and water densities are the average values obtained from the Ocean Drilling Program (ODP) Leg 155, Sites 937B, 938A and 939B (Flood et al., 1995). These sites were chosen because, among the 17 sites in this leg, they are the closest ones in terms of water depth to our study region (site 937B is at 2760 mwd, site 938A is at 2804 mwd and site 939B is at 2792 mwd). A fixed porosity of 76% for $0 \leq Z \leq 1.1$ m and variable porosity as a function of depth for $Z > 1.1$ m, were defined following the ODP Leg 155, Sites 937B, 938A and 939B data, based on the porosity values for those sites (Fig. 3). The thermal conductivity (1.07 W/m.K) and the geothermal heat flow (28 mW/m^2) are average values for those three sites, determined based on the work of Pribnow et al. (2000). In their work, there is no distinction between a "wet" and a "dry" thermal conductivity (both required for the model input); however, considering the values of "wet" thermal conductivity used in other modelling studies, which range between 1.0 and 1.4 W/m.K (Thatcher et al., 2013; Marín-Moreno et al., 2013, 2015a, 2015b; Stranne, O'Regan and Jakobsson, 2016, 2017), the value of 1.07 W/m.K was established as the "wet" thermal conductivity. Here, the "wet" thermal conductivity refers to the sediment conductivity under fully water-saturated conditions. For further information, see the TOUGH + HYDRATE User's Manual (Moridis and Pruess, 2014; Moridis, 2014).

For the LGM, we considered that the sea level was 123 m below the current level and that the BWTs were 4.3 °C lower than the current values, based on the data of Waelbroeck et al. (2002) for the North Atlantic Ocean. The curves of sea level and BWT increase since the LGM up to the present were also determined from the data of Waelbroeck et al. (2002) for the North Atlantic Ocean (Fig. 4). It is worth noting that the data of Waelbroeck et al. (2002) were derived from cores recovered in a northernmost region on the North Atlantic Ocean (around 55°N 14°W), in water depths around 2200 m. Although the conditions in this region are certainly different than those of our study area (around 4°10′S 49°15′W – Fig. 1, water depths between 550 and 750 m), we assume that the data are applicable to our study area, for lack of better sources.

The current BWTs were determined for each water depth considered as average values, taken from Ketzer et al. (2018, Fig. 1B). The temperatures at the LGM were then determined subtracting 4.3 °C from the current BWTs values, as shown in Table 2. With the BWTs at the LGM

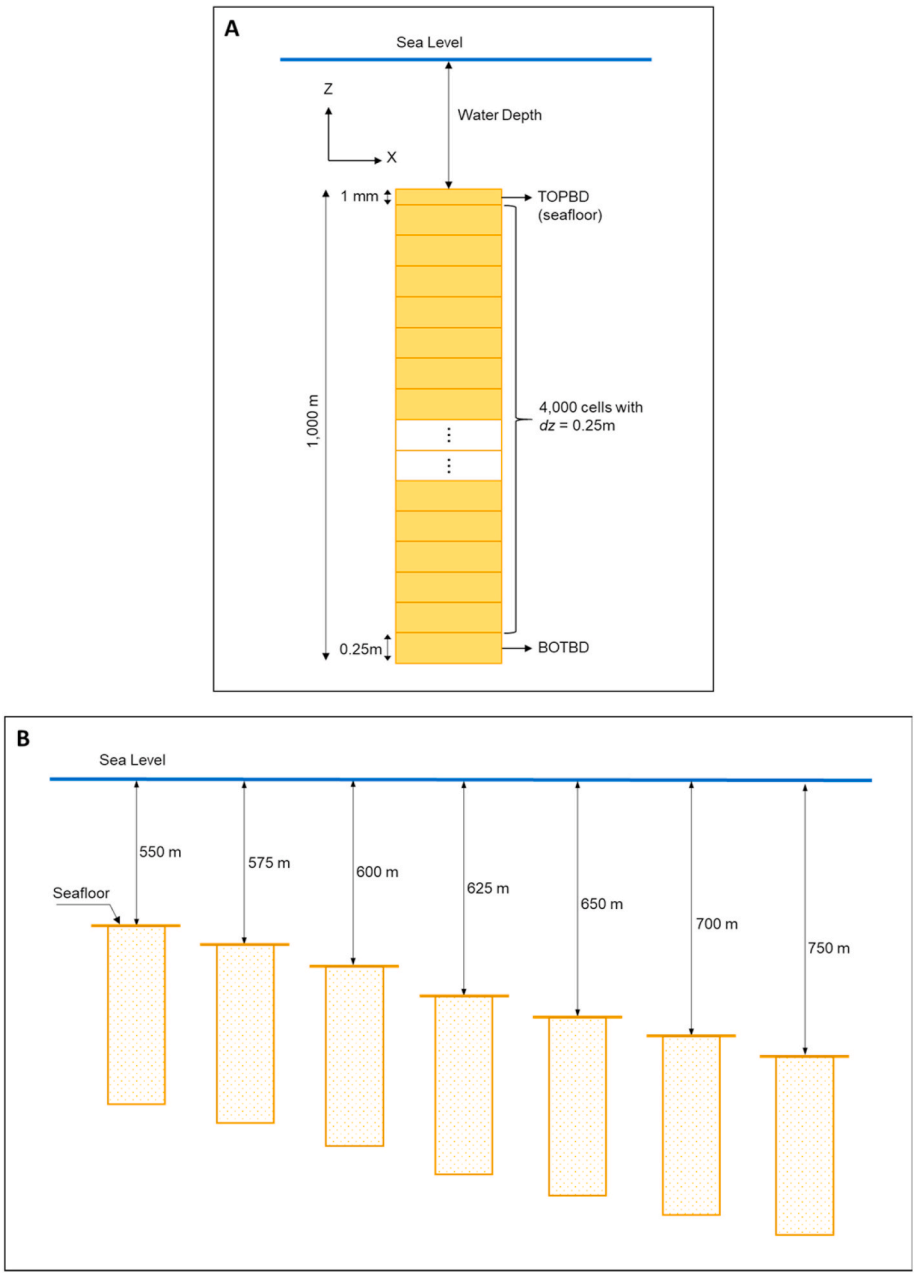

Fig. 2. (**A**) Vertical 1D model scheme (TOPBD = top boundary; BOTBD = bottom boundary). (**B**) Schematic representation of the basic 1D model at 550, 575, 600, 625, 650, 700 and 750 mwd (not to scale).

obtained for each water depth considered and converting the sea level into hydrostatic pressure, we constructed the curves of pressure and temperature increase, since the LGM up to the present (Fig. 5). Because the data of Waelbroeck et al. (2002) are limited up to 500 y BP, it was assumed that the sea level and the BWTs have remained constant in the last 500 years.

Prior to the simulations of simultaneous pressure and BWTs variation, each 1D model was initialized with hydrostatic pressure distribution, temperature distribution for a constant basal heat flow of 28 mW/m^2 and initial methane hydrate saturation of 3%, homogeneously distributed within the MHSZ (Table 1). In the initialization, we used the conditions for the LGM, i.e., sea level at 123 m below the current level, and BWTs 4.3 °C lower than the current values. At the end of this initialization process, the models were in steady state (constant pressure and temperature, and no mass fluxes). To distribute the temperature in the models, at the LGM, with the basal heat flow of 28 mW/m^2, it was assumed that the heat flow has not changed in the study area in the last 20,000 years.

After the initialization of each model, we performed the simultaneous pressure and BWTs variation simulations, since the LGM up to the present. To do so, we defined the pressure and the temperature increases as functions of time (Fig. 5) in the top cell of each model.

It is worth noting that, in the initialization of the models, we did not consider neither gaseous methane under the MHSZ, nor basal gaseous methane fluxes. Thus, the gaseous methane fluxes at the seafloor recorded during the simulations and the corresponding cumulative masses of gaseous methane released into the ocean are sourced from the methane hydrate dissociation itself only. We also did not consider neither the presence of the sulfate reduction zone, nor the anaerobic oxidation of methane, since they are out of the scope of this study. With this assumption, methane hydrates were present at the LGM (initial condition) immediately below the seafloor with the 3% saturation

Table 1
Properties and simulations parameters.

Property	Value	Reference
Salinity	0.035 kg/kg	Average value from ODP Leg 155, Sites 937B, 938A and 939B[a]
Water density	1024 kg/m^3	
Sediment grain density	2726 kg/m^3	
Porosity ∅	For $0 \leq z \leq 1.1$ mbsf, $\varphi = 76\%$ For $z > 1.1$ mbsf, $\varphi = f(z)$	From ODP Leg 155, Sites 937B, 938A and 939B[a]
Basal heat flow	28 mW/m^2	Average value from ODP Leg 155, Sites 937B, 938A and 939B, (Pribnow et al., 2000)[b]
Wet Thermal Conductivity	1.07 W/m.K	
Dry Thermal conductivity	0.55 W/m.K	Marín-Moreno et al. (2015a, 2015b)
Grain specific heat	1000 J/kg°C	T + H User's Manual v1.5 (Moridis, 2014)
Initial Hydrate Saturation	3%	Klauda and Sandler (2005); Reagan and Moridis (2008)
Permeability	1×10^{-15} m^2 (1mD)	Average value from Reagan and Moridis (2008); Thachter et al., 2013; Stranne et al., 2016a,b, 2017.
Methane hydrates formation/ dissociation model	Equilibrium	T + H User's Manual v1.5 (Moridis, 2014)
Pore Compressibility	0.00 (initialization runs) 1.0×10^{-8} Pa^{-1} (pressure and BWTs increases, since the LGM up to the present)	This study T + H User's Manual v1.5 (Moridis, 2014)
Composite Thermal Conductivity λ_θ	$\lambda_\theta = \lambda_{dry} + (\sqrt{S_A} + \sqrt{S_H})(\lambda_{wet} - \lambda_{dry})$	T + H User's Manual v1.5 (Moridis, 2014)
Relative permeability (k_r) model: Modified version of Stone's first three-phase relative permeability method	$k_{rA} = \left[\frac{S_A - S_{irA}}{1 - S_{irA}}\right]^n$, $k_{rG} = \left[\frac{S_G - S_{irG}}{1 - S_{irG}}\right]^{n_G}$ $S_{irA} = 0.20$; $S_{irG} = 0.02$; $n = n_G = 4$	Stone (1970) in TOUGH + Core Code v1.5 User's Manual (Moridis and Pruess, 2014). Parameters from Reagan and Moridis (2008)
Capillary pressure (P_{cap}) model: van Genuchten Function	$P_{cap} = -P_0[(S^*)^{-1/\gamma} - 1]^{1-\gamma}$ $S^* = \frac{(S_A - S_{irA})}{(S_{mxA} - S_{irA})}$, $-P_{max} \leq P_{cap} \leq 0$ $\gamma = 0.45$; $S_{irA} = 0.19$; $P_0 = 2,000\ Pa$ $P_{max} = 10^6\ Pa$; $S_{mxA} = 1.0$	Van Genuchten (1980) in TOUGH + Core Code v1.5 User's Manual (Moridis and Pruess, 2014). Parameters "γ", "S_{irA}" and "P_0" are from Reagan and Moridis (2008), and "P_{max}" and "S_{mxA}" are from Thatcher et al. (2013)
Method for "k_r" and "P_{cap}" estimation in the presence of solid phases	Original Porous Medium, no scaling of capillary pressure: [MOP(8) = 9]	TOUGH + Core Code v1.5 User's Manual (Moridis and Pruess, 2014)

[a] Data of the ODP Leg 155, Sites 937B, 938A and 939B are available at <http://www-odp.tamu.edu/publications/155_SR/COREDATA/CORE.HTM#Hole%20937>.

[b] Data from Pribnow et al. (2000) for ODP Leg 155, Sites 937B, 939A and 939B are available at <http://www-odp.tamu.edu/publications/heatflow/>

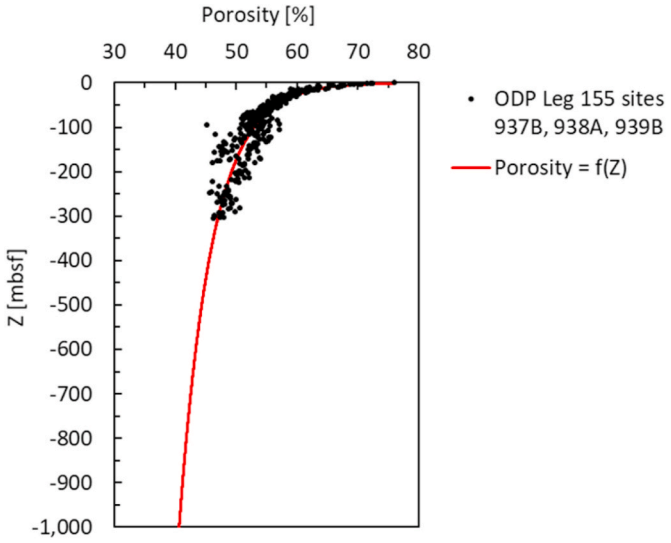

Fig. 3. Porosity curve (red) obtained from the porosity values as a function of the depth below the seafloor for the ODP Leg 155, Sites 937B, 938A and 939B (black dots) (mbsf = meters below seafloor) (data available at www-odp.tamu.edu/publications/155_SR/COREDATA/CORE.HTM#Hole%20,937). (For interpretation of the references to colour in this figure legend, the reader is referred to the Web version of this article.)

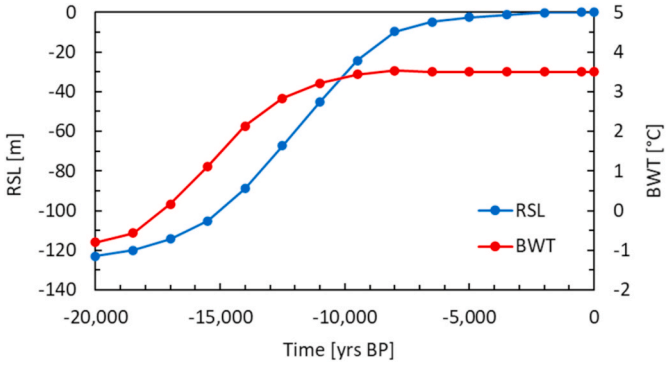

Fig. 4. Relative sea level (RSL) and bottom water temperature (BWT) variation over the last 20,000 years. Data from Waelbroeck et al. (2002), available at <www.ncdc.noaa.gov/paleo-search/study/10496>.

Table 2
Bottom water temperatures (BWTs) in the present and in the LGM.

Water depth [m]	BWT in the present [°C] (average values from Ketzer et al., 2018 – Fig. 1B)	BWT in the LGM [°C] ($BWT_{present}$ – 4.3 °C)
550	7.1	2.8
575	6.9	2.6
600	6.6	2.3
625	6.4	2.1
650	6.2	1.9
700	5.9	1.6
750	5.5	1.2

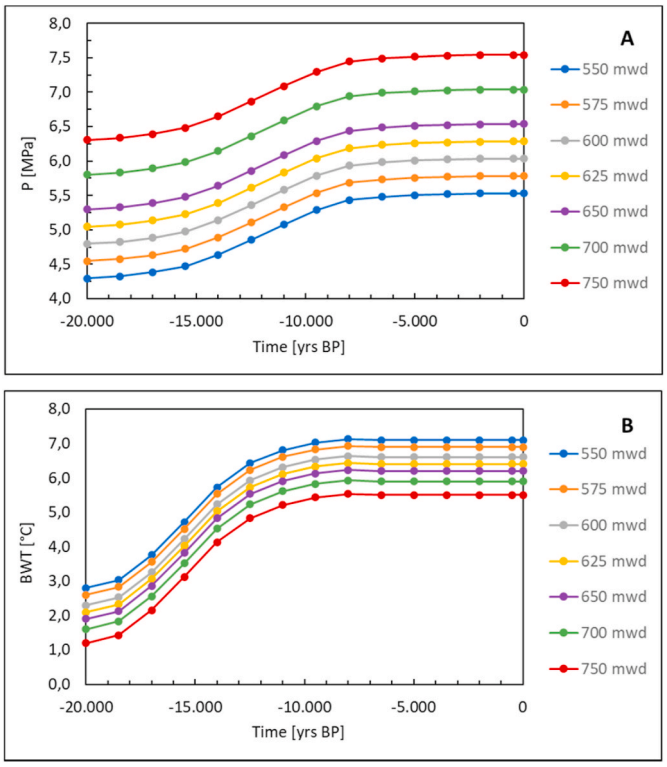

Fig. 5. Sea bottom pressure (**A**) and BWTs (**B**) increase curves, since the LGM up to the present, for each water depth considered in this study. The curves were constructed based on the data from Waelbroeck et al. (2002), converting the sea level values into pressure.

considered. Because the anaerobic oxidation of methane is not considered, the gaseous methane from hydrate dissociation is released into the ocean if it reaches the seafloor.

3. Results

During the simulations, the gaseous methane fluxes at the seafloor and the corresponding cumulative masses of gaseous methane released into the ocean were calculated, as well as the amount of methane hydrates within each model, as functions of time. These fluxes are the maximum possible fluxes, since no other sinks for methane such as AOM are considered. For each model, the methane hydrate saturation (S_H) and the gas saturation (S_G), as functions of the depth Z below the seafloor at different times were also calculated. Because methane hydrates can only occur within the MHSZ, the evolution with time of hydrate saturation as a function of depth reflects the evolution of the stability zone in each model. The amount of hydrate, gas fluxes through the seafloor and cumulative mass of gaseous methane released into the ocean over time are presented in Figs. 6–8, respectively. The evolution with time of S_H and S_G as functions of the depth below the seafloor are available as video animations in the supplementary material for this work.

When the pressure and the BWTs start to increase after the beginning of the simulations, opposite effects start to take place in the MHSZ, because an increase in pressure tends to increase the stability zone, while an increase in temperature tends to reduce it. When the MHSZ starts to shrink, hydrate dissociation begins, releasing water and gaseous methane into the sediment pores, resulting in an increase in S_G and in a decrease in S_H, and in the amount of hydrate within the system.

The results show that, for the shallowest water depths considered (550 and 575 mwd), the MHSZ vanishes during the simulation period, resulting in the dissociation of all the methane hydrate initially present in the models around 12,000–15,000 y BP (Fig. 6 and videos S1 and S2). This indicates that, at this point, the decrease in hydrate stability caused by the BWTs increases has completely overcome the stability enhancement caused by the pressure increase. Part of the gaseous methane that was released during hydrate dissociation flowed into the ocean, resulting in ~110 kg/m^2 and ~100 kg/m^2 of gaseous methane released into the ocean, for 550 and 575 mwd, respectively (Figs. 7 and 8). For these two depths, in the present, there are gaseous methane fluxes at the seafloor (Fig. 7), and gaseous methane is present close to the seafloor and at several meters below it (videos S1 and S2). Thus, gaseous methane might still be released into the ocean for years and even decades, for 550 and 575 mwd. However, our results do not allow to confirm or rule out this possibility, because a significant part of the methane may be consumed by AOM within the SRZ, which were not accounted for in this work.

Supplementary video related to this article can be found at https://doi.org/10.1016/j.marpetgeo.2021.105494

For the other water depths considered, the response of the methane hydrate to the simultaneous pressure and BWTs increases was less "dramatic". The results show that, for 600, 625, 650, 700 and 750 mwd, although the MHSZ has shrank, leading to hydrate dissociation and gaseous methane release into the sediment pores, it has not disappeared completely (Fig. 6 and videos S3 to S7). This indicates that, for these water depths, the decrease in the methane hydrate stability caused by the BWTs increases has only partly overcome the stability enhancement due to pressure increase. For 600 mwd, gaseous methane was released into the ocean only between 14,000 and 7000 y BP (Fig. 7), resulting in ~30 kg/m^2 of gaseous methane released into the ocean over that period (Fig. 8). For the other water depths (625, 650, 700 and 750), no gaseous methane was released into the ocean during the simulations (Figs. 7 and 8). For the water depths in which gaseous methane has been continuously released into the ocean since ca. 17,500 y BP (550 and 575 mwd), and in which gaseous methane was released into the ocean between ca. 14,000 and 7000 y BP (600 mwd) (Figs. 7 and 8), hydrate dissociated both at the base and at the top of the MHSZ (videos S1, S2 and S3). However, for the other water depths (where no gaseous methane release was observed), methane hydrate dissociated only at the base of the MHSZ (videos S4 to S7). This indicates that, where hydrate dissociated only at the base of the MHSZ, gaseous methane was not released into the ocean. On the other hand, where hydrate dissociated at the top of the MHSZ, gaseous methane could reach the seafloor (if not consumed by oxidation) and gas release into the ocean was observed.

Regarding the behavior of the hydrate stability zone, the results indicate that it has shrank at the end of the simulation, in all the water depths considered, in response to the simultaneous pressure and BWTs changes. Fig. 9 shows, for each water depth considered, the depth (below the seafloor) of the base of the MHSZ, in the LGM and in the present. The reduction in the stability zone was greater for the shallower water depths, (completely vanished in the present for both 550 and 575 mwd, as previously indicated). Analyzing Fig. 9, it is possible to speculate that the decrease in the MHSZ tends to be progressively smaller for greater water depths. Indeed, a simple extrapolation performed with the variation of the base of the stability zone for 650, 700 and 750 mwd indicate that the MHSZ would not decrease for water depths of ~900 m and greater, given the conditions used in this study.

4. Discussion

An important feature of the simultaneous sea level (pressure) and BWTs increases is the opposite effects that they have on methane hydrate stability. As already mentioned, an increase in sea level favors hydrate stability, while an increase in temperature reduces it. This was one of the motivations to perform the simulation of simultaneous pressure and BWT variation. In our models, for shallow water depths, the effect of the BWTs increases has completely overcome the effect of sea level increase on hydrate stability. This result, however, may be related to the sea level and BWTs, which have offset increase curves (Figs. 4 and

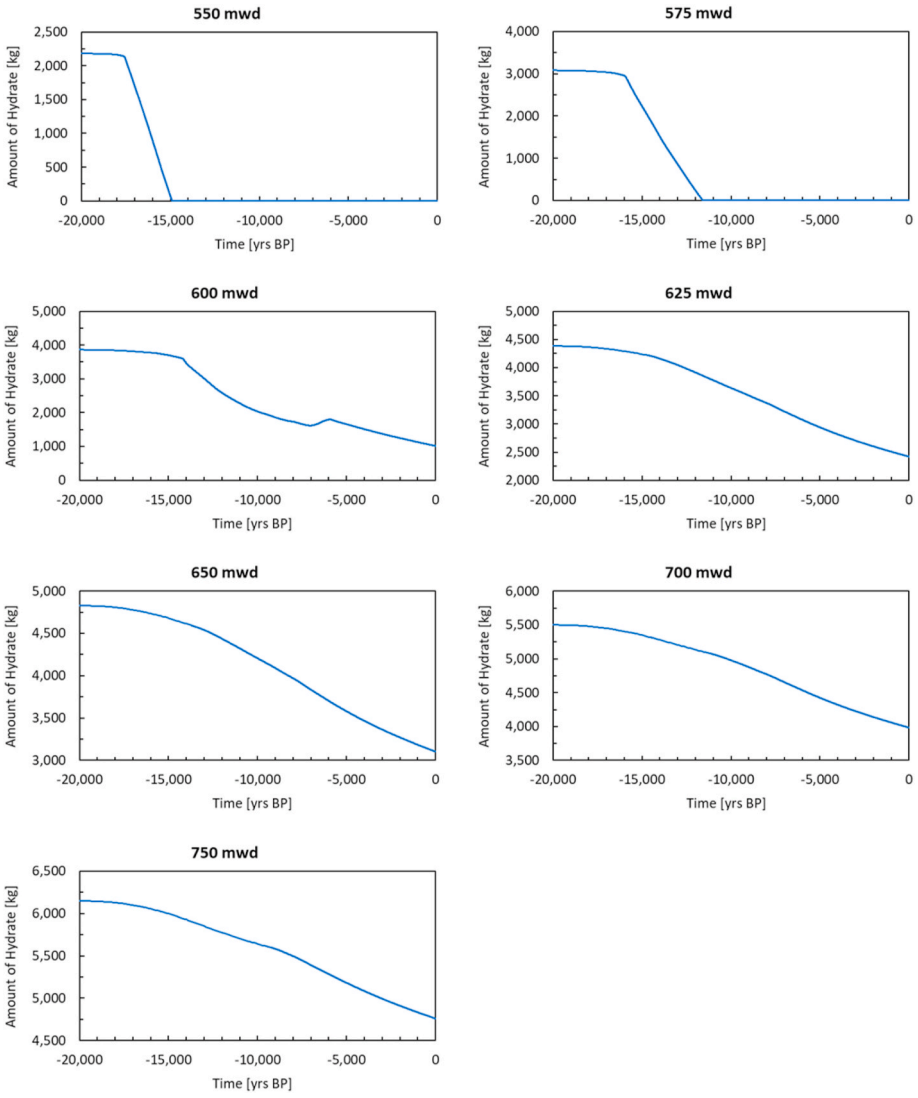

Fig. 6. Amount of methane hydrate in each model as a function of time.

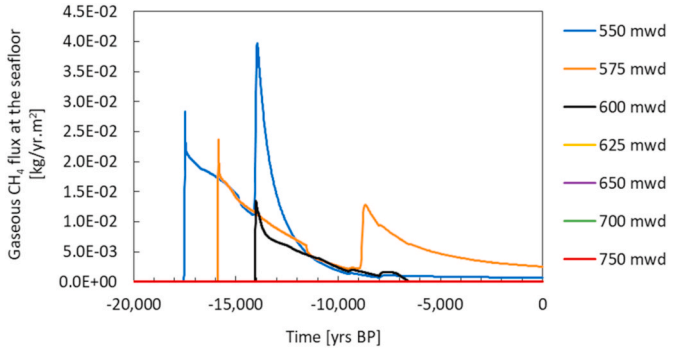

Fig. 7. Gaseous CH_4 flux at the seafloor as a function of time, for each model. (Curves for 625 mwd, 650 mwd, 700 mwd and 750 mwd are coincident and shown in red). (For interpretation of the references to colour in this figure legend, the reader is referred to the Web version of this article.)

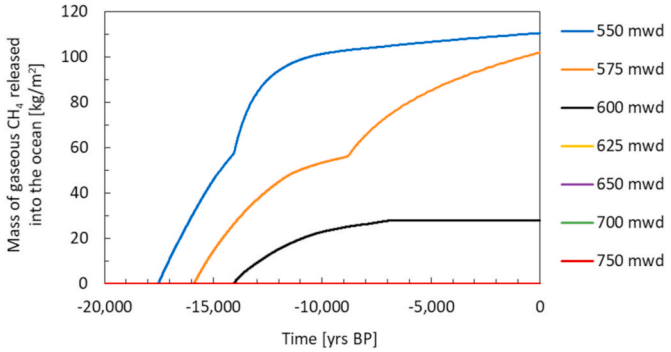

Fig. 8. Cumulative mass of gaseous CH_4 released into the ocean, for each model. (Curves for 625 mwd, 650 mwd, 700 mwd and 750 mwd are coincident and shown in red). (For interpretation of the references to colour in this figure legend, the reader is referred to the Web version of this article.)

5). During deglaciation, temperatures rose sooner, triggering the melting of ice sheets later in the early Holocene – ca. 12,000 y BP.

One of the striking features of the Amazon Fan is the presence of giant mass-transport deposits (MTDs) (Maslin et al., 2005). Maslin et al. (2005) suggest that the glacial MTDs referred to as Deep Eastern MTD and Unit R MTD may be linked to gas hydrate dissociation, since these periods correlate with rapid sea level drop. According to the authors, the Deep Eastern MTD occurred between 35,000 and 37,000 y BP and the Unit R MTD occurred about 41,000–45,000 y BP. On the other hand, the authors suggest that the deglacial MTDs referred to as Western and

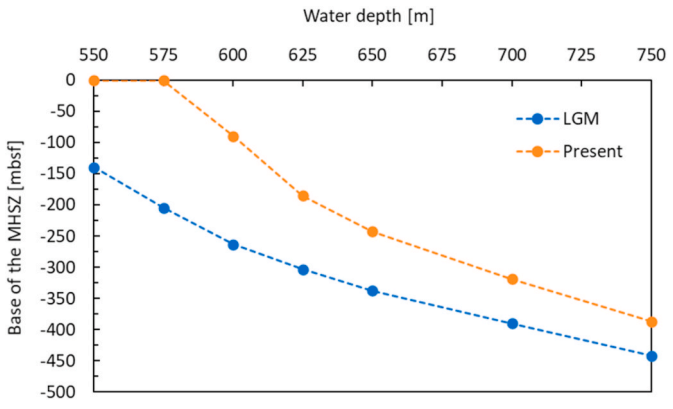

Fig. 9. Depth (below the seafloor) of the base of the MHSZ in the LGM and in the present, for each water depth considered (mbsf = meters below seafloor). Note that, in the present, there is no MHSZ for 550 and 575 mwd.

Eastern Debris Flows, that occurred between 13,000 and 14,000 y BP, may not be related to gas hydrate dissociation, because the sea level rose rapidly during that period. It is argued that a rapid increase in intermediate water temperatures that would overcome the effect of sea level rise is unlikely, since the transmission of temperature changes from the seafloor to the base of the MHSZ is very slow, and because there is no evidence of such a rapid intermediate water temperature increase on the Amazon Fan. Our results contradict this hypothesis from Maslin et al. (2005) and suggest another scenario. If the sea level and the BWTs increase curves adopted are applicable to the study area on the Amazon Fan, the effect of the BWTs increase may have completely overcome the effect of the sea level increase on the methane hydrate stability, for shallow water depths (550 and 575 mwd). This phenomenon may have caused dramatic methane hydrate dissociation between 15,000 and ~12,000 y BP for those two water depths (Fig. 6). Rapid methane releases may have caused seafloor instability and triggered slope failures. However, to confirm this hypothesis, it would be necessary to couple flow and transport simulations performed here with a geomechanical model.

On the Amazon Fan, gas plumes have been recently detected in the water column, covering water depths from 650 to 2600 m (Ketzer et al., 2018). The plumes between 650 and 715 mwd may be related to gas hydrate dissociation, since they occur within the current depth range of the feather edge of the MHSZ (Ketzer et al., 2018, 2019). According to our results, gaseous methane released during hydrate dissociation driven by simultaneous sea level and BWTs increases over the last 20,000 years, is venting on the seafloor, in the present, at 550 and 575 mwd, but not at greater water depths. Therefore, our results would suggest that gaseous methane from hydrate dissociation due to simultaneous pressure and BWTs increases since the LGM up to the present would not have contributed to the gas plumes detected and reported by Ketzer et al. (2018), between 650 and 715 mwd. If this is correct and if these gas plumes are indeed related to gas hydrate dissociation, then other causes would be required to explain hydrate dissociation and gas release into the ocean, for example, seasonal BWTs oscillations (e.g., Braga et al., 2020) and/or BWTs increases over the last decades or centuries, caused by global warming (e.g., Reagan and Moridis, 2008). It is worth noting, however, that our results contain a lot of uncertainties due to inevitably less-constrained input data (e.g., BWTs in the present and in the LGM, pressure and temperature variations in the region during the period, and initial methane hydrate saturation), and due to the assumptions and simplifications adopted in our models (e.g., no methane recharge during the simulations). Furthermore, it was assumed that the BWTs remained constant in the last 500 years (Section 2). Thus, it would not be prudent to rule out the possibility that the gas plumes detected between 650 and 715 mwd would have received the contribution of gas released during hydrate dissociation driven by sea level and BWTs increases, since the LGM up to the present.

As already mentioned, we did not consider neither the sulfate reduction zone (SRZ), nor the anaerobic oxidation of methane (AOM) in this work. It means that: (1) initially (i.e., at the LGM), methane hydrates were present immediately below the seafloor in each model, and (2) all the gaseous methane from hydrate dissociation that reached the seafloor was released into the ocean. By disregarding this microbial methane filter (Egger et al., 2018; Stranne et al., 2019), the cumulative masses of gaseous methane released into the ocean for 550, 575 and 600 mwd (~110 kg/m^2, ~100 kg/m^2 and ~30 kg/m^2, respectively – Fig. 8) may have been overestimated. If we consider that 90% of the methane produced in ocean sediments is consumed by AOM, as reported by Stranne et al. (2019), then only ~11 kg/m^2, ~10 kg/m^2 and ~3 kg/m^2 of gaseous methane would have been released into the ocean for 550, 575 and 600 mwd, respectively, since the LGM up to the present. Although we can speculate about cumulative masses of gaseous methane released into the ocean if the AOM had been accounted for, it is not possible to speculate how gaseous methane fluxes on the seafloor (Fig. 7) would have evolved with time if AOM had been considered. AOM is a dynamic and complex process, which may be related to several processes that occur in marine sediments. Egger et al. (2018) suggested that sedimentation rates and the associated organic carbon burial rates exert a key control on the depth of the sulfate-methane transition (also referred to as sulfate-methane interface, that lies at the base of the SRZ – e.g., Rodrigues et al., 2017). The results of the modelling study performed by Stranne et al. (2019) indicated that the AOM efficiency depends on the oxidation rate and on the sediment permeability evolution (formation of fractures). Thus, to investigate the effects of AOM on methane releases into the ocean, since the LGM up to the present, a complex study would be carried out, which should account for oxidation rates, sedimentation rates, permeability evolution and formation of fractures. However, our results allow the comparison of the relative amount of gaseous methane release in different water depths, as well as the relative amount of hydrate that dissociated in the last 20,000 years.

5. Conclusions

We performed numerical simulations to investigate the dynamic response of shallow methane hydrates to simultaneous sea level (pressure) and BWTs increases, since the LGM up to the present, on the Amazon Deep-Sea Fan, Amazonas Basin, Equatorial Atlantic Ocean, Brazil. The simulations were performed with seven 1D models representative of seven water depths: 550, 575, 600, 625, 650, 700 and 750 m. The initial conditions for each model referred to the LGM and, since we did not consider neither gaseous methane under the MHSZ, nor basal fluxes of gaseous methane in the models, we could investigate gaseous methane release into the ocean only due to methane hydrate dissociation itself.

The results suggest that: (1) The methane hydrate stability decrease caused by the early BWT increase during the simulated period has completely overcome the stability enhancement due to sea level increase, for 550 and 575 mwd. On the other hand, hydrate stability decrease caused by the BWT increase has only partly overcome the stability enhancement due to sea level increase, for the other water depths considered (600, 625, 650, 700 and 750 mwd). (2) For 550 and 575 mwd, the stability zone has completely vanished in the models and all the methane hydrate initially present has dissociated. Gaseous methane started to be released into the ocean at ca. 17,500 y BP for 550 mwd and at ca. 16,000 y BP for 575 mwd. (3) For 600 mwd, the MHSZ shrank during the simulation, but did not disappear. Hydrate dissociated and part of the gaseous methane that was released during hydrate dissociation flowed into the ocean only between 14,000 and 7000 y BP. The gaseous methane that did not reach the ocean stayed below the remaining MHSZ. (4) For 625, 650, 700 and 750 mwd, the MHSZ has also shrunk, but did not disappear as well. However, all the gaseous methane that was released during hydrate dissociation remained below

the MHSZ and thus, no gaseous methane was released into the ocean in these models. Because we did not consider the anaerobic oxidation of methane, the magnitude of the gaseous methane fluxes at the seafloor may be considered as maximum possible values, and the time in which they occurred in the past may have been different.

Despite some inevitably less-constrained input data and simplifications adopted, this conceptual study contributes to improve the understanding of methane hydrate dynamics when subjected to simultaneous sea level (pressure) and BWTs increases, within a multiphase and multicomponent approach, for which there is a lack of published studies. Furthermore, our results can be used as initial conditions for further studies.

Declaration of competing interest

The authors declare that they have no known competing financial interests or personal relationships that could have appeared to influence the work reported in this paper.

Acknowledgements

This work was developed in the Institute of Petroleum and Natural Resources (IPR), at the Pontifical Catholic University of Rio Grande do Sul – PUCRS, Porto Alegre, Brazil. We thank Profs. Drs. Jorge Hugo Silvestrini and Rubem Mário Figueiró Vargas, from the Post-Graduation Program, and Dr. João Marcelo Ketzer for their valuable comments, as well as for their help during the development of this work. This study was financed in part by the Coordenação de Aperfeiçoamento de Pessoal de Nível Superior - Brasil (CAPES) - Finance Code 001.

References

Braga, R., Iglesias, R.S., Romio, C., Praeg, D., Miller, D.J., Viana, A., Ketzer, J.M., 2020. Modelling methane hydrate stability changes and gas release due to seasonal oscillations in bottom water temperatures on the Rio Grande cone, offshore southern Brazil. Mar. Petrol. Geol. 112 https://doi.org/10.1016/j.marpetgeo.2019.104071.

Darnell, K.N., Flemings, P.B., 2015. Transient seafloor venting on continental slopes from warming-induced methane hydrate dissociation. Geophys. Res. Lett. 42 (10) https://doi.org/10.1002/2015GL067012, 765-10,772.

Egger, Matthias, Riedinger, Natascha, Mogollón, José M., Jørgensen, Bo Barker, 2018. Global diffusive fluxes of methane in marine sediments. Nat. Geosci. 11, 421–425. https://doi.org/10.1038/s41561-018-0122-8.

Flood, R.D., Piper, D.J.W., Klaus, A., et al., 1995. Proceedings of the Ocean Drilling Program. Initial Reports, Vol. 155. Chapters available at: http://www-odp.tamu.edu/publications/155_IR/155TOC.HTM.

Hester, Keith C., Brewer, Peter G., 2009. Clathrate hydrates in nature. Ann. Rev. Mar. Sci 1, 303–327. https://doi.org/10.1146/annurev.marine.010908.163824.

Hunter, S.J., Goldobin, D.S., Haywood, A.M., Ridgwell, A., Rees, J.G., 2013. Sensitivity of the global submarine hydrate inventory to scenarios of future climate change. Earth Planet Sci. Lett. 367, 105–115.

Ketzer, J.M., Augustin, A., Rodrigues, L.F., Oliveira, R., Praeg, D., Pivel, M.A.G., Reis, A. T., Silva, C., Leonel, B., 2018. Gas seeps and gas hydrates in the Amazon deep-sea fan. Geo Mar. Lett. 38, 429–438. https://doi.org/10.1007/s00367-018-0546-6.

Ketzer, Marcelo, Praeg, Daniel, Pivel, Maria A.G., Augustin, Adolpho H., Rodrigues, Luiz F., Viana, Adriano R., Cupertino, José A., 2019. Gas seeps at the edge of the gas hydrate stability zone on Brazil's continental margin. Geosciences 9 (5), 193. https://doi.org/10.3390/geosciences9050193.

Ketzer, M., Praeg, D., Rodrigues, L.F., Augustin, A., Pivel, M.A.G., Rahmati-Abkenar, M., Miller, D.J., Viana, A.R., Cupertino, J.A., 2020. Gas hydrate dissociation linked to contemporary ocean warming in the southern hemisphere. Nat. Commun. 11, 3788. https://doi.org/10.1038/s41467-020-17289-z.

Klauda, Jeffery B., Sandler, Stanley I., 2005. Global distribution of methane hydrate in ocean sediment. Energy Fuels 19, 459–470. https://doi.org/10.1021/ef049798o.

Marín-Moreno, H., Minshull, T.A., Westbrook, G.K., Sinha, B., Sarkar, S., 2013. The response of methane hydrate beneath the seabed offshore Svalbard to ocean warming during the next three centuries. Geophys. Res. Lett. 40, 5159–5163. https://doi.org/10.1002/grl.50985.

Marín-Moreno, H., Minshull, T.A., Westbrook, G.K., Sinha, B., 2015a. Estimates of future warming-induced methane emissions from hydrate offshore west Svalbard for a range of climate models. G-cubed 16, 1307–1323. https://doi.org/10.1002/2015GC005737.

Marín-Moreno, H., Giustiniani, Michela, Tinivella, Umberta, 2015b. The potential response of the hydrate reservoir in the South Shetland Margin, Antarctic Peninsula, to ocean warming over the 21st century. Polar Res. 34 (1), 27443. https://doi.org/10.3402/polar.v34.27443.

Maslin, Mark, Vilela, Claudia, Mikkelsen, Naja, Grootes, Pieter, 2005. Causes of catastrophic sediment failures of the Amazon Fan. Quat. Sci. Rev. 24, 2180–2193. https://doi.org/10.1016/j.quascirev.2005.01.016.

Moridis, G.J., Pruess, K., 2014. User's Manual of the TOUGH+ Core Code v1.5: A General-Purpose Simulator of Non-isothermal Flow and Transport through Porous and Fractured Media. Lawrence Berkeley National Laboratory, California.

Moridis, G.J., 2014. User's Manual for the HYDRATE v1.5 Option of TOUGH+ v1.5: A Code for the Simulation of System Behavior in Hydrate-Bearing Geologic Media. Lawrence Berkeley National Laboratory, California.

Paull, C.K., Ussler III, W., Dillon, W.P., 1991. Is the extent of glaciation limited by marine gas-hydrates? Geophys. Res. Lett. 18, 432–434.

Phrampus, B.J., Hornbach, M.J., 2012. Recent changes to the Gulf Stream causing widespread gas hydrate destabilization. Nature 490.

Pribnow, Daniel, Kinoshita, Masataka, Stein, Carol, 2000. Thermal Data Collection and Heat Flow Recalculations for Ocean Drilling Program Legs 101-180. Available at: http://www-odp.tamu.edu/publications/heatflow/.

Reagan, M.T., Moridis, G.J., 2007. Oceanic gas hydrate instability and dissociation under climate change scenarios. Geophys. Res. Lett. 34, 1–5. https://doi.org/10.1029/2007GL031671.

Reagan, M.T., Moridis, G.J., 2008. Dynamic response of oceanic hydrate deposits to ocean temperature change. J. Geophys. Res. 113, C12023. https://doi.org/10.1029/2008JC004938.

Reagan, M.T., Moridis, G.J., Elliott, S.M., Maltrud, M., 2011. Contribution of oceanic gas hydrate dissociation to the formation of Arctic Ocean methane plumes. J. Geophys. Res. 116, C09014. https://doi.org/10.1029/2011JC007189.

Rodrigues, Luiz Frederico, Ketzer, João Marcelo, Lourega, Rogério Véscia, Augustin, Adolpho Herbert, Sbrissa, Gesiane, Miller, Dennis, Heemann, Roberto, Viana, Adriano, Freire, Antonio Fernando Menezes, Morad, Sadoon, 2017. The influence of methane fluxes on the sulfate/methane Interface in sediments from the Rio Grande Cone Gas Hydrate Province, southern Brazil. Braz. J. Genet. 47 (3), 369–381. https://doi.org/10.1590/2317-4889201720170027.

Sloan, Dendy, 2003. Fundamental principles and applications of natural gas hydrates. Nature 426, 353–359. https://doi.org/10.1038/nature02135.

Stranne, C., O'Regan, M., Dickens, G.R., Crill, P., Miller, C., Preto, P., Jakobsson, M., 2016a. Dynamic simulations of potential methane release from East Siberian continental slope sediments. G-cubed 17. https://doi.org/10.1002/2015GC006119.

Stranne, C., O'Regan, M., Jakobsson, M., 2016b. Overestimating climate warming-induced methane gas escape from the seafloor by neglecting multiphase flow dynamics. Geophys. Res. Lett. 43, 8703–8712. https://doi.org/10.1002/2016GL070049.

Stranne, C., O'Regan, M., Jakobsson, M., 2017. Modeling fracture propagation and seafloor gas release during seafloor warming-induced hydrate dissociation. Geophys. Res. Lett. 44, 8510–8519. https://doi.org/10.1002/2017GL074349.

Stranne, Christian, O'Regan, Matt, Jakobsson, Martin, Brüchert, Volker, Ketzer, Marcelo, 2019. Can anaerobic oxidation of methane prevent seafloor gas escape in a warming climate? Solid Earth 10, 1541–1554. https://doi.org/10.5194/se-10-1541-2019.

Thatcher, K.E., Westbrook, G.K., Sarkar, S., Minshull, T.A., 2013. Methane release from warming induced hydrate dissociation in the West Svalbard continental margin: timing, rates, and geological controls. J. Geophys. Res. Solid Earth 118, 22–38. https://doi.org/10.1029/2012JB009605.

Tréhu, A.M., Ruppel, C., Holland, M., Dickens, G.R., Torres, M.E., Collett, T.S., Goldberg, D., Riedel, M., Schultheiss, P., 2006. Gas hydrates in marine sediments: lessons from scientific ocean drilling. Oceanography 19 (4), 124–142. https://doi.org/10.5670/oceanog.2006.11.

Waelbroeck, C., Labeyrie, L., Michel, E., Duplessy, J.C., McManus, J., Lambeck, K., Balbon, E., Labracherie, M., 2002. Sea-level and deep water temperature changes derived from benthic foraminifera isotopic records. Quat. Sci. Rev. 21, 295–305. Tabulated data available in. https://www.ncdc.noaa.gov/paleo-search/study/10496.

Xu, Wenyue, Lowell, Robert P., Peltzer, Edward T., 2001. Effect of seafloor temperature and pressure variations on methane flux from a gas hydrate layer: comparison between current and late Paleocene climate conditions. J. Geophys. Res. 106 https://doi.org/10.1029/2001JB000420. B11, 26,413-426,423.